



**HAL**  
open science

## **Sn(TFSI) 2 as Suitable Salt For the Electrodeposition of Nanostructured Cu<sub>6</sub>Sn<sub>5</sub> - Sn Composite obtained on Cu electrode in Ionic Liquid**

Nadia Soulmi, Ana-Gabriela Porras-Gutierrez, Natalia Mordvinova, Oleg Lebedev, Cécile Rizzi, Juliette Sirieix-Plenet, Frédéric Lantelme, Henri Groult, Damien Dambournet, Laurent Gaillon

### ► To cite this version:

Nadia Soulmi, Ana-Gabriela Porras-Gutierrez, Natalia Mordvinova, Oleg Lebedev, Cécile Rizzi, et al.. Sn(TFSI) 2 as Suitable Salt For the Electrodeposition of Nanostructured Cu<sub>6</sub>Sn<sub>5</sub> - Sn Composite obtained on Cu electrode in Ionic Liquid. *Inorganic Chemistry Frontiers*, 2019, 6 (1), pp.248-256. 10.1039/C8QI00982A . hal-02182286

**HAL Id: hal-02182286**

**<https://hal.sorbonne-universite.fr/hal-02182286v1>**

Submitted on 12 Jul 2019

**HAL** is a multi-disciplinary open access archive for the deposit and dissemination of scientific research documents, whether they are published or not. The documents may come from teaching and research institutions in France or abroad, or from public or private research centers.

L'archive ouverte pluridisciplinaire **HAL**, est destinée au dépôt et à la diffusion de documents scientifiques de niveau recherche, publiés ou non, émanant des établissements d'enseignement et de recherche français ou étrangers, des laboratoires publics ou privés.

# Sn(TFSI)<sub>2</sub> as Suitable Salt For the Electrodeposition of Nanostructured Cu<sub>6</sub>Sn<sub>5</sub>-Sn Composite obtained on Cu electrode in Ionic Liquid

Nadia Soulmi,<sup>a</sup> Ana-Gabriela Porras-Gutierrez,<sup>\*a,c</sup> Natalia E. Mordvinova,<sup>b</sup> Oleg I. Lebedev,<sup>b</sup> Cécile Rizzi,<sup>a,c</sup> Juliette Sirieix-Plénet,<sup>a,c</sup> Frédéric Lantelme,<sup>a,c</sup> Henri Groult,<sup>a,c</sup> Damien Dambournet,<sup>a,c</sup> and Laurent Gaillon <sup>\*a,c</sup>

The preparation of binder and carbon-free electrodes is of great interest owing to higher energy density. In this scope, electrodeposition is a suitable method that can be easily scale up providing that suitable chemical reactants are used. In this work, we used highly soluble Sn precursor based on TFSI counter ion dissolved in [EMIm][TFSI] ionic liquid. The use of similar anionic groups in both Sn precursor and solvent allowed to avoid impurities typically encountered when using Sn chloride precursor. The resulting solution was characterized by cyclic voltametry using either inert (Mo) and reactive substrate (Cu). In both cases, the electrodeposition occurred in a diffusion controlled process. In the case of Cu, however, a Cu-Sn alloy that is  $\eta$ -Cu<sub>6</sub>Sn<sub>5</sub> phase was identified. A FIB cross section revealed that Cu and Sn interdiffused and that no epitaxial growth occurred. Prolonging the electrodeposition time favored the formation of  $\beta$ -Sn because Cu could no longer diffuse within the deposited structure. This resulted in a mixed  $\beta$ -Sn/ $\eta$ -Cu<sub>6</sub>Sn<sub>5</sub> composite whose proportions depended on the deposition duration time. The deposited samples were directly assembled in lithium coin cells to characterize the capacity and cyclability of binder and carbon-free electrodes. Increasing the mass of deposited sample degraded the capacity and reversibility of the system which was explained by a lower ability to accommodate the volume variation occurring during the electrochemical lithiation/delithiation process.

## Introduction

Sn-based materials are challenging the practical widely used graphite anode materials for Li-ion batteries because of their higher lithium storage capacity (up to 991 mAh g<sup>-1</sup> for a Li<sub>4.4</sub>Sn composition). However, due to dramatic volume expansion (up to approximately 300 %) during the charge/discharge cycling, Sn-based electrode provides only poor cycle life caused by its mechanical disintegration.<sup>1,2</sup>

Downscaling the size of the material is one approach of choice to overcome this issue by buffering these expansion/contraction processes.<sup>3,4</sup> However to reach higher conductivity between the grains without loss of mechanical properties, several strategies associated to electrode formulation, embedding and processing have been used.<sup>5</sup> Sn/C based composites electrode, with high binder content (to maintain adhesion to the current collector and cohesion within the composite) is currently required to rise good electrochemical performances.<sup>6,7</sup> Likewise considerable interest have also been given to intermetallic Sn-based materials, where an inactive metal M vs. Li<sup>+</sup>/Li was used to modulate the volume change (e.g. M =Cu, Ni, Co, Fe, etc.).<sup>8-11</sup>

Instead of composite electrode, the use of pure metallic Sn electrode could be employed by combining nanostructuring with a thin film approach.<sup>12-13</sup>

Such electrodes can be obtained more easily by an electrodeposition process that uses an electric field to reduce ionic species onto a specific substrate. Typically, the deposition of metallic species can be performed directly on a collector of current with the advantages that tuning the experimental conditions (i.e. solvent, electrode substrate, applied potential or current density, metallic

salt precursor, additives, working temperature, etc.) permit to modulate the morphology of the deposit.<sup>14</sup>

Henceforth, electrodeposition in ionic liquids (ILs) media is of great interest owing to their wide electrochemical potential window stability, high deposition current efficiency and furthermore, compared to conventional aqueous electrolyte the deposit does not suffer from H<sub>2</sub> evolution and metal oxide formation.<sup>15,16</sup>

It has already been demonstrated that Sn can be electrodeposited from various ILs electrolytic solutions,<sup>17</sup> among which imidazolium<sup>18</sup> and pyrrolidinium<sup>19</sup> based ionic liquids solutions are most often used. Electrodeposition of Sn has also been achieved from ILs mixture with AlCl<sub>3</sub>,<sup>20,21</sup> or ZnCl<sub>2</sub>,<sup>22</sup> or even in deep eutectic solvent.<sup>23</sup>

Even if experimental deposition conditions modulate the morphology, the thickness, and the nanostructuring of the deposited layer, in this kind of synthesis, they are also dramatically influenced by the choice of the anion/cation combination of the IL.<sup>19,24-27</sup> Indeed the physicochemical properties of the solvent (conductivity, solubility, viscosity) impact the deposition potentials and the electrodeposition mechanism. In the case of Sn deposit, some studies have already underline the influence of the anion <sup>24,26-29</sup> through viscosity and stabilization of the precursor tin species from one part. From another part, the influence of the ionic liquid cation through viscosity and likely its different adsorption /interactions with the substrate or the nuclei was also demonstrated <sup>26-28</sup>. Different complexes of Sn<sup>2+</sup> with various ILs have been identified by infrared spectroscopy, also underlining that both anion and cation of the IL play a role in the deposition process.<sup>26</sup>

One of the main drawback when using ILs for Sn electrodeposition is the low solubility of the generally used

halide precursor salt ( $\text{SnCl}_2$ ).<sup>30</sup> Moreover, the anhydrous salt should be privileged rather than its stable hydrated form (*i.e.*  $\text{SnCl}_2 \cdot 2\text{H}_2\text{O}$ ) since water is undesired in the electrolytic media. Al-Salman *et al.*<sup>28</sup> showed that the liquid (but very hygroscopic) solution of  $\text{SnCl}_4$  could also be used. Otherwise, when using  $\text{SnCl}_2$ , due to its strong donor ligand properties [ $\text{DCA}^-$ ] (dicyanamide) anion based ILs were demonstrated to provide highest solubility of this metal salt precursor,<sup>31–33</sup> and therefore has been thoroughly studied for Sn electrodeposition. [ $\text{DCA}^-$ ] anion is generally associated to [ $\text{EMIm}^+$ ] (1-ethyl-3-methylimidazolium) cation because this IL has a low viscosity and high conductivity.<sup>26,27,31</sup>

Therefore, ILs with [ $\text{TFSI}^-$ ] (bis(trifluoromethanesulfonyl) imide) anion are generally preferred because they are known for their low hydrophilicity and hence low water uptake compared to [ $\text{DCA}^-$ ] anion, low viscosity and good conductivity. But through the fact that [ $\text{TFSI}^-$ ] is a non-coordinating anion, such ILs suffer from low solubility of halide salts. In one of our previous study, to overcome this issue, we had used anodic electrodisolution of a metallic Sn wire to introduce the desired amount of  $\text{Sn}^{2+}$  in the solution.<sup>27</sup> One of the additional benefits of this method was that neither halides nor other counter ions were introduced in the electroplating bath. Therefore, the electrogenerated  $\text{Sn}^{2+}$  cations could only complex with the anion of the IL used.

In the present study, [ $\text{EMIm}^+$ ][ $\text{TFSI}^-$ ] IL was used to prepare solutions incorporating  $\text{Sn}(\text{TFSI})_2$  salt, as plating solutions to electrodeposit Sn nanostructures. The salt  $\text{Sn}(\text{TFSI})_2$  was chosen because of its good solubility in ILs composed with the same counter-anion. Sn nanostructures obtained directly on the current collector (active copper substrate), when varying electrodeposition conditions (duration, potential, concentration of Sn precursor) were shown to influence the electrochemical performances (charge/discharge capacity and cycling stability) of such a synthesized binder-free negative electrode.

## Experimental

### Chemicals.

1-Ethyl-3-methylimidazolium bis(trifluoromethanesulfonyl) imide ([ $\text{EMIm}^+$ ][ $\text{TFSI}^-$ ]), 99.5% and the electrolyte 1M lithium hexafluorophosphate in ethylene carbonate : ethyl methyl carbonate (1:1 vol.%) with 2%wt. fluoroethylene carbonate were obtained from Solvionic.  $\text{Sn}(\text{II})$  bis(trifluoromethyl sulfonyl)imide ( $\text{Sn}(\text{TFSI})_2$ ) was obtained from Alfa Aesar, and the acetonitrile (ACN), HPLC grade 99.9 %, was obtained from Sigma-Aldrich.

All the chemical were used as received and stored in glove box filled with argon ( $\text{H}_2\text{O}$  and  $\text{O}_2$  content < 1 ppm).

### Preparation and electrochemical characterization of Sn electrodes.

All electrochemical measurements were performed in the glove box filled with argon ( $\text{H}_2\text{O}$  and  $\text{O}_2$  content < 1 ppm). A three-

electrodes electrochemical cell controlled by a potentiostat (PAR 273A) was used. Cu ( $A = 0.785 \text{ cm}^2$ ) or Mo ( $A = 0.503 \text{ cm}^2$ ) foils were used as working electrode (they were cleaned with 1M  $\text{H}_2\text{SO}_4$  solution, rinsed with water and dried prior to uses). The counter electrode was a Pt wire and a Sn bar was used as reference electrode.

Cyclic voltammetry (CV) curves were recorded at different scanning rates ( $0.005 - 0.200 \text{ Vs}^{-1}$ ) in an electrochemical window between  $-0.6$  and  $+0.4 \text{ V vs. Sn}^{2+}/\text{Sn}$ .

The electrodeposition of Sn was performed potentiostatically at  $-0.3 \text{ V vs. Sn}^{2+}/\text{Sn}$  for a given duration. After the deposition, the samples were thoroughly cleaned in the glove box to avoid oxidation of the surface, with acetonitrile to remove all the IL present at the surface of the electrode.<sup>34</sup>

### Characterization Methods.

The X-ray diffraction (XRD) was performed using a Rigaku Ultima IV X-ray diffractometer with a  $\text{Cu K}\alpha$  radiation ( $\lambda = 1.54059 \text{ \AA}$ ) with a scan rate of  $0.1^\circ \text{ min}^{-1}$  between  $10^\circ$  and  $80^\circ$  ( $2\theta$ ).

Scanning Electron Microscopy (SEM) measurements were performed with a SEM-FEG ZEISS ultra 55 equipped with or coupled to a Bruker QUANTAX EDS analysis system.

The microstructure of the Sn-based electrode was examined with transmission electron microscopy (TEM). Two type of TEM samples were prepared. The first one was obtained by scrapping the electrode surface and further depositing the material together with ethanol on holey Ni holey carbon grid. In order to investigate substrate/film interface and possible interdiffusion, cross-section samples were prepared by focused ion beam (FIB) techniques in Helios Nano Lab 660FIB. Electron diffraction (ED) and high resolution TEM (HRTEM) experiments were performed on Tecnay G2 30 UT microscope operated at 300 kV and having 0.17 nm point resolution. High angle annular dark field scanning TEM (HAADF-STEM) imaging and energy dispersive x-ray spectroscopy (EDX) elemental mapping were recorded on a double aberration corrected JEM ARM200F cold FEG electron microscope operated at 200 kV and equipped with large solid-angle CENTURIO EDX detector.

### Electrochemical Characterization.

The electrochemical performances as negative electrode material in Li-ion battery of the as-prepared Sn-based electrodes were carried out with CR2032-type coin cells. The electrolyte was 1 M  $\text{LiPF}_6$  dissolved in a mixture of ethylene carbonate (EC) and ethyl methyl carbonate (EMC) (1:1 vol. %) with 2%wt. of fluoroethylene carbonate (FEC). The cells were assembled with lithium metal as the anode and were tested in the voltage range of  $2.0 - 0.05 \text{ V vs. Li}^+/\text{Li}$  at different current densities.

## Results and Discussion

**Cyclic voltammetry study using inert (Mo) and reactive (Cu) electrodes.**

A solution containing Sn(TFSI)<sub>2</sub> solubilized in [EMIm<sup>+</sup>][TFSI<sup>-</sup>] was characterized to investigate the electrochemical behaviour using two different working electrodes that are copper and molybdenum. Cu is commonly used as a current collector for negative electrode materials. It is, therefore, an interesting substrate for Sn electrodeposition as it allows to prepare an electrode ready to be used in a lithium cell. However, it can form alloys with Sn at room temperature which makes it a reactive substrate/electrode.<sup>35–37</sup> On the other hand, Mo does not form alloys with Sn and is therefore a non-reactive substrate suitable to characterize the electrochemical behaviour of Sn<sup>2+</sup> in solution.

Cyclic voltammetry was used to characterize the electrochemical properties of a 25 mM solution of Sn(TFSI)<sub>2</sub> in [EMIm<sup>+</sup>][TFSI<sup>-</sup>]. **Figure 1** presents the cyclic voltammograms obtained using Mo and Cu as working electrodes at a scan rate of 0.05 Vs<sup>-1</sup> starting from the open current potential (E<sub>OCp</sub>) toward cathodic and reversed anodic sides. The potential window was -0.6 to +0.4 V which is within the electrochemical stability window of [EMIm<sup>+</sup>][TFSI<sup>-</sup>] ionic liquid (Supporting Information, **Figure S1**) The E<sub>OPC</sub> was around +0.2 V. In both electrode materials, the shape of the reduction peak is characteristic of an electrodeposited solid that is insoluble.<sup>38</sup>

On Mo electrode, a cathodic peak was observed at -0.17 V vs. Sn<sup>2+</sup>/Sn and was assigned to the reduction of Sn<sup>2+</sup> to Sn<sup>0</sup>. On the reverse potential scan, Sn was re-oxidized at around +0.10 V. The current loop during the cathodic and the anodic scan indicated that the electrodeposition of Sn into Mo required an overpotential to initiate nucleation and growth, as already observed in diverse ILs.<sup>19,27</sup>

On the Cu electrode, the reduction peak appeared at a potential of -0.08 V, which was higher than that observed in Mo electrode. Moreover, the loop feature observed in the case of Mo was absent here. This meant that Cu electrode did not require an over potential to initiate growth of Sn due the interaction between Sn and the substrate. After the first reduction peak, the current still decreased smoothly which might indicate the occurrence of other chemical reactions coupled to the primary electrochemical process and/or the formation of others composition of Sn-Cu alloys. The occurrence of these additional reactions was also suggested by the ratio of the total anodic to cathodic charge (Q<sub>a</sub>/Q<sub>c</sub>) which was lower than unity indicating that the deposited material was not totally electrochemically removed during the positive scan.

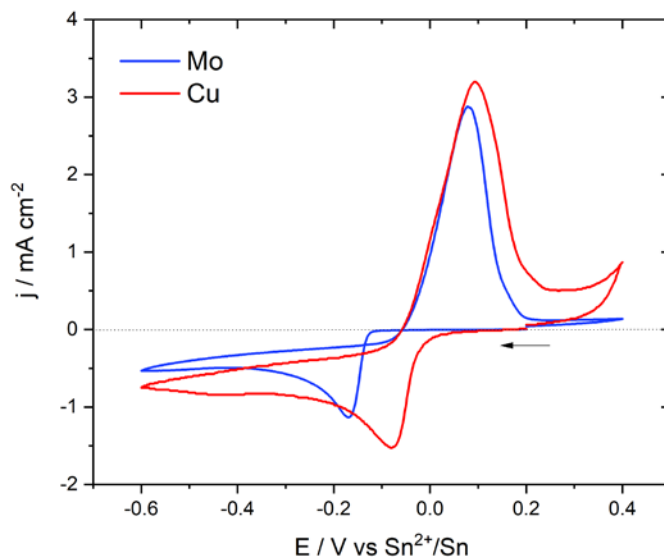


**Figure 1.** Cyclic voltammetry of 25 mM Sn(TFSI)<sub>2</sub> in [EMIm<sup>+</sup>][TFSI<sup>-</sup>] on Cu and Mo electrodes at a scan rate of 0.05 Vs<sup>-1</sup>.

Cyclic voltammetry was performed at different scan rates. On the Mo electrode (**Fig. 2a**), an increase of the scan rate led to an increase of the over-potential. In contrast, the oxidation peak remained relatively unchanged. Due to the overpotential electrocrystallisation, it was difficult to compare and to interpret the variation of  $\Delta E_p = E_{pa} - E_{pc}$  in terms of reversibility or irreversibility of the reaction.

On the Cu electrode (**Fig. 2b**), the reduction peak potential did not vary significantly with an increasing scan rate. For all scan rates, the reduction current started at the equilibrium potential of the redox couple. The overvoltage at the zero-crossing,  $\eta_0 = -0.05V$ , of backward curves was close to its theoretical value predicted for reversible systems.<sup>39,40</sup>

The CVs, overall, indicated an electrochemical behaviour largely influenced by the nature of the working electrode. However, a linear relationship between the cathodic peak current density and the square root of the scan rate ( $I_{pc} = f(v^{1/2})$ ), in Mo and Cu electrodes, indicated that the reduction of Sn<sup>2+</sup> were governed by diffusion-controlled processes<sup>8,41,42</sup> (Figure S2) as follows :

$$I_{pc} = -0.6104nFAC_0^* \sqrt{\frac{nF}{RT} v D_{Sn^{2+}}} \quad (1)$$

where  $I_{pc}$  is the current intensity of the cathodic peak,  $C_0^*$  the concentration of the electroactive species and  $D_{Sn^{2+}}$  the diffusion coefficient of the Sn<sup>2+</sup> species. It should be noted that both plots did not pass through the origin. The non-zero intercept may be assigned to an adsorption phenomena and some surface chemical coupled reactions.<sup>29,43</sup> The diffusion coefficient of Sn<sup>2+</sup> species,  $D_{Sn^{2+}}$  can be determined

according to equation (1) for a reversible (diffusion-controlled) deposition process on a massive electrode. Because Cu

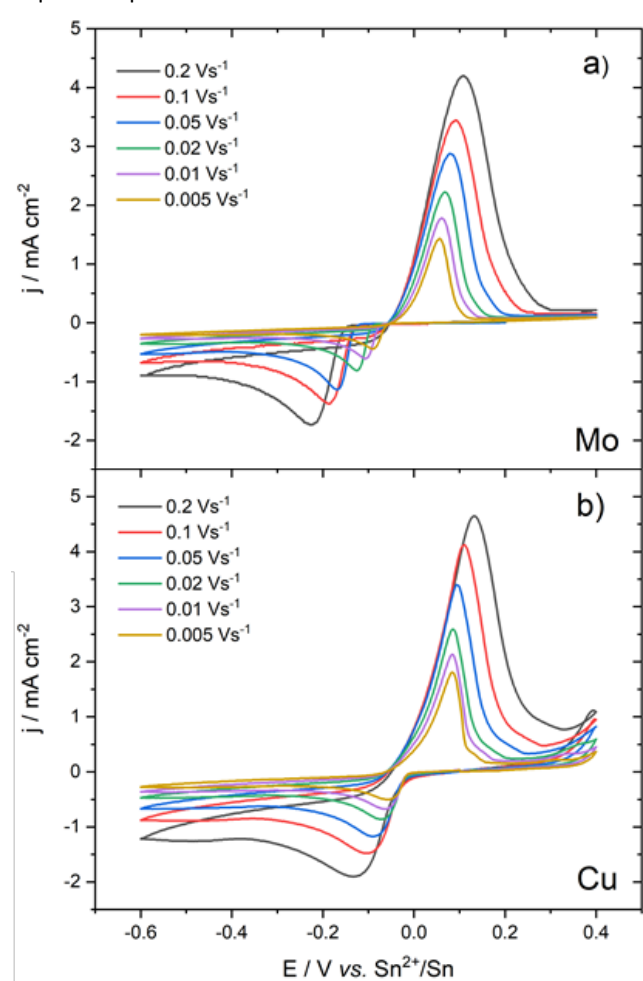


**Figure 2.** Evolution of the cyclic voltammograms of a 25 mM  $\text{Sn}(\text{TFSI})_2$  in  $[\text{EMIm}^+][\text{TFSI}^-]$  solution at different scan rates on a) Mo, and b) Cu electrodes.

electrode formed alloys with Sn species, the  $D_{\text{Sn}^{2+}}$  calculation was not possible using equation 1, while Mo electrode offered the suitable non-reactive surface.

The calculated diffusion coefficient of  $\text{Sn}^{2+}$  species in  $[\text{EMIm}^+][\text{TFSI}^-]$  at 298 K in Mo electrode was approximately  $1.61 \times 10^{-8} \text{ cm}^2 \text{ s}^{-1}$ . The  $D_{\text{Sn}^{2+}}$  in  $[\text{EMIm}^+][\text{TFSI}^-]$  is in the same order of magnitude than that reported in  $[\text{EMIm}^+][\text{BF}_4^-]$ ,  $[\text{EMIm}^+][\text{TfO}^-]$ ,<sup>29</sup> and  $[\text{BMP}^+][\text{TFSI}^-]$ .<sup>19,30</sup> However, it is lower than those determined in  $[\text{EMIm}^+][\text{DCA}^-]$  and  $[\text{BMP}^+][\text{DCA}^-]$ ,<sup>27,29,30</sup> probably due to higher viscosity for  $[\text{EMIm}^+][\text{TFSI}^-]$  that induced a lower mobility of  $\text{Sn}^{2+}$ . Moreover, because the coordination state of  $\text{Sn}^{2+}$  is modified by the counter ion solvation force of the ionic liquid anion versus the counter-ion of Sn precursor, different solvation environments influencing  $\text{Sn}^{2+}$  mobility are expected.

#### Electrodeposition and characterization of deposited solids.

To better understand the reactivity of  $\text{Sn}^{2+}$  on the Cu electrode, a cathodic deposition was performed at -0.3 V, a potential located after the reduction peak, in the mass-transfer controlled region for different duration times (5 min, 30 min, 1h and 2h). In such experiments, the mass of deposited solid scales linearly with the time of the electrodeposition (**Figure S3**). In general, the use of ILs as electrolyte prevents the occurrence of side reactions and therefore allows high efficiency to be obtained.<sup>15</sup> Increasing the duration time led to an increasing amount of deposited solids as revealed by the colour changes of the substrate going from black for lower mass to bright metallic for higher deposited mass (**Figure S4**). Moreover, all samples showed good adhesion to the substrate.

XRD measurements were performed on the deposited solids obtained at different duration times (**Figure 3**). Overall, the XRD patterns of the electrodeposited solids could be indexed with two phases exhibit Bragg peaks characteristic of  $\beta\text{-Sn}$  (space group:  $I41/amd$ ) and  $\eta\text{-Cu}_6\text{Sn}_5$  (space group:  $P63/mmc$ ). Prolonging the duration time led to an intensity increase of the [200] and [101] lines of  $\beta\text{-Sn}$ . At  $t > 1\text{h}$ ,  $\beta\text{-Sn}$  became the predominant phase suggesting that  $\eta\text{-Cu}_6\text{Sn}_5$  was formed at the early stage of the deposition and then, once Cu and Sn could no longer interdiffuse,  $\beta\text{-Sn}$  started to form. This was confirmed by energy-dispersive X-ray (EDX) spectroscopy measurements and associated Sn/ Cu ratio that showed that increasing the deposition time led to an increasing and decreasing contents of Sn and Cu, respectively (**Figure S5**).

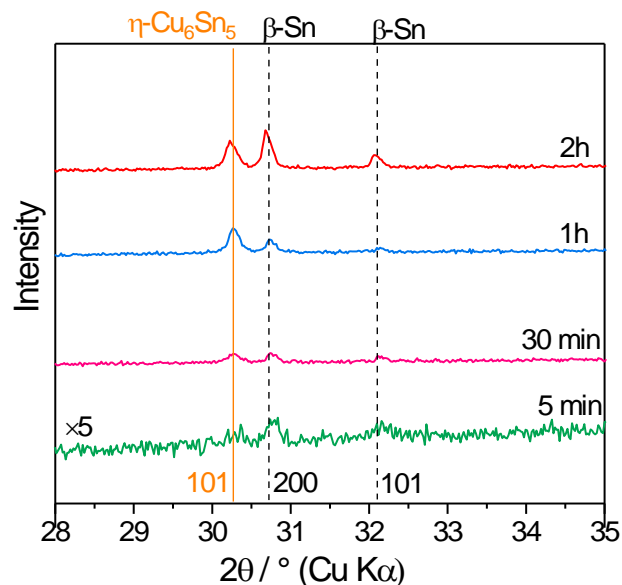


**Figure 3.** XRD patterns performed on electrodeposited samples obtained at different deposition times.

To extend the comprehension on the formation of Cu-Sn alloy, a FIB cross section TEM sample of a Cu electrode was prepared on which a solid was electrodeposited during 30 min. HAADF-STEM image of the corresponding cross section is shown

in **Figure 4a**. It shows that the electrodeposited solid was not uniformly attached to the Cu substrate and quite uneven at nanoscale level. High resolution HAADF-STEM image (**Figure 4b**)

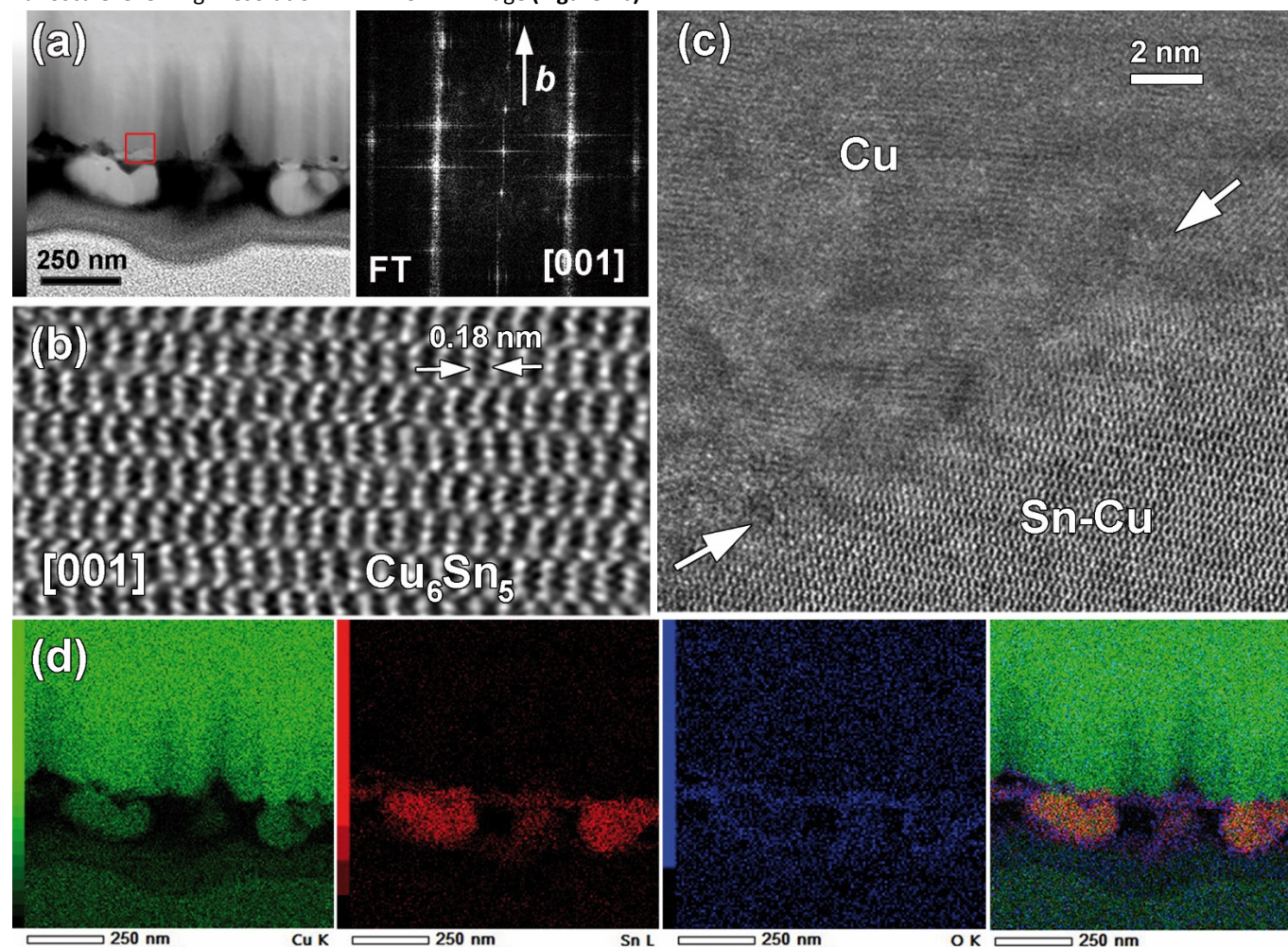


**Figure 4.** a) Low magnification HAADF-STEM image of FIB cross section of a Cu electrode on which a solid was electrodeposited during 30 min. b) High resolution [001] HAADF-STEM image of single grain showing  $\eta$ - $\text{Cu}_6\text{Sn}_5$  phase and corresponding FT pattern given above c) HAADF-STEM image showing the interface between the Cu electrode and electrodeposited solid marked in (a) by red square (arrows). d) EDX elemental mapping of Cu K (green), Sn L (red), O K (blue) and overlaid colour map.

was obtained on single [001] oriented grain and allowed to identify the  $\eta$ - $\text{Cu}_6\text{Sn}_5$  phase which was further confirmed by corresponding FT pattern. In **Figure 4c**, high-resolution HAADF-STEM image of Cu/deposited solid interface did not evidence any epitaxial growth between the substrate and the deposited solid. This suggested that Cu and Sn interdiffused to form the  $\eta$ - $\text{Cu}_6\text{Sn}_5$  phase. EDX elemental mappings shown in **Figure 4d** revealed that Sn was present both at the surface of the Cu electrode and within larger grains, *i.e.*, around 200 nm. The HAADF-STEM image and Cu K mapping clearly showed the occurrence of attachment point from which these large particles were growth. This highlighted the diffusion of Cu coming from the substrate.

The morphology at the particle level was investigated by HAADF-STEM imaging and EDX mapping on particles obtained

by scraping the surface of the Cu electrodes. Typical examples of TEM images along with EDX mapping of the particles observed are shown in **Figure 5a**. For all samples, we observed particles featuring two different sizes, small ones in the range of 3-15 nm and larger ones with sizes ranging from 100-300 nm after 5 min, 200-400 nm after 30 min, 300-1000 nm after 1h and 200-800 nm after 2h. EDX mapping performed on the samples obtained after 5 min and 2h of deposition, revealed the presence of both Sn and Cu at the particle level. In the case of the 5 min deposition, we observed generally a homogenous distribution of Sn and Cu, in agreement with the predominant formation of  $\eta$ - $\text{Cu}_6\text{Sn}_5$  phase. However, small areas of Sn-O phase could also be observed. In the case of the 2h deposition, we observed Cu and Sn separation. While Sn was present all over the particle, Cu was not (see SI **Figure S6** for other

examples), which was in agreement with the formation of  $\beta$ -Sn as shown by XRD analysis. The formation of two phases was also

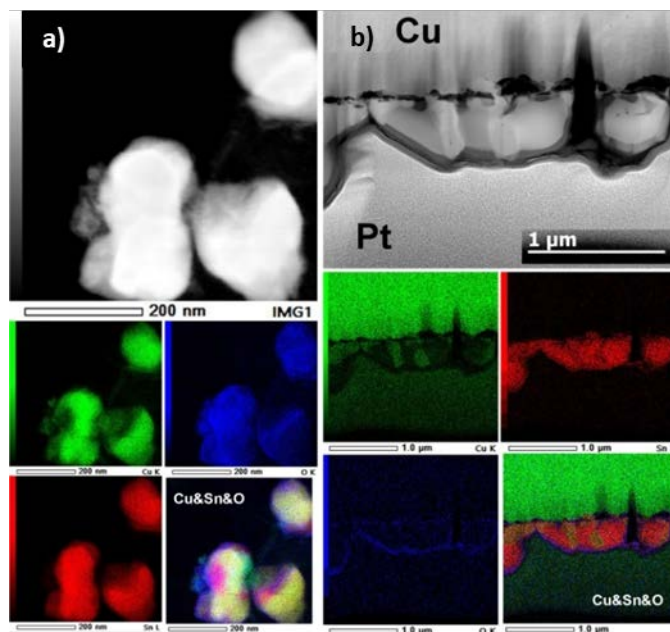
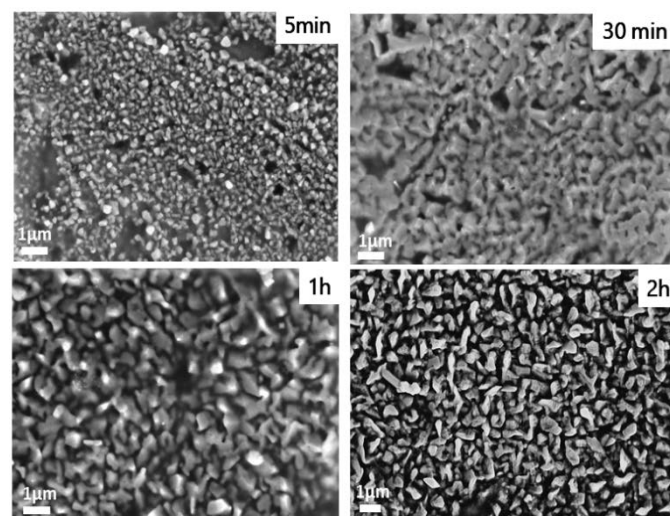


**Figure 5.** a) HAADF-STEM image of the particles obtained by scrapping the electrode surface obtained on the electrodeposited solids for 5 min and corresponding EDX elemental mapping of Cu K(green), Sn L(red), O K(blue) and overlaid colour image. b) HAADF-STEM image of FIB sample of a Cu electrode on which a solid was electrodeposited during 2h and corresponding EDX elemental mapping of Cu K(green),Sn L(red), O K(blue) and overlaid colour image .

Scanning electron microscopy was further used to visualize the upper scale of the particle's organization (**Figure 6**). After 5 min of deposition, the solid is composed of nanoparticles. After 30 min and 1h, a network of interconnected particles was observed. This interconnected organization disappears after 2h of deposition suggesting a different growth mechanism.



confirmed by EDX mapping performed on a cross section for a sample prepared for 2h (**Figure 5b**).

**Figure 6.** Scanning electron micrographs of the electrodeposited samples prepared at different duration time.

The occurrence of interconnected particles might be caused by the interdiffusion of Cu and Sn. For longer duration time, however, Cu atoms cannot reach the top of the deposited surface leaving the growth of Sn particles forming isolated structures.

#### Electrochemical properties.

The electrodeposited solids on Cu substrate provided electrode materials free of carbon and binder additives. They were directly assembled in coin-type half cells to investigate their properties vs.  $\text{Li}^+/\text{Li}$ .

The multi-step lithiation/delithiation processes on Sn electrode<sup>3,29,44</sup> as on Sn based alloy electrode<sup>29,45-48</sup> are already well documented, and it has already been concluded that CV profiles and peak potentials are in both cases characteristic of electrodes containing metallic tin. Especially the plateau of potential attributed to the lithiation of  $\text{Cu}_6\text{Sn}_5$  arise in the same domain of potential where intermetallic tin-lithium phases prevail. The potentials of the peaks in charge are similar in both cases to Sn-Li de-alloying process. Comparison of CV curves obtained on electrodes with lower and higher amounts of tin (**Figure S7**) does not permit to distinguish the composition of the electrode.

**Figure 7** presents the galvanostatic discharge/charge curves obtained on the series of electrodeposited samples. The mass of the active materials determined by the measured current during the electrodeposition process yielded 0.04 mg for 5 min, 0.085 mg for 30 min, 0.15 mg for 1h and 0.29 mg for 2h. Cells were cycled between 0.05 V and 2.0 V (vs.  $\text{Li}^+/\text{Li}$ ) at a current density of  $100 \text{ mA g}^{-1}$ .

During the first discharge, all the samples featured an irreversible plateau at around 1.5 V vs.  $\text{Li}^+/\text{Li}$ . Such a plateau was also observed in other studies and was assigned to the decomposition of the electrolyte (EC degradation) and the formation of the solid electrolyte interface (SEI) layer.<sup>49</sup> We noted that the plateau length decreased with the increase of the deposition duration time. The occurrence of isolated nanoparticles obtained after 5 min might favour the decomposition of the electrolyte due to higher surface area.

During the first cycle, all samples presented a large irreversible capacity. The charge capacity decreased with the increase of the deposition duration time with the corresponding values obtained for the first charge of : 900 (5 min), 400 (30 min), 265 (1h) and 190 (2h)  $\text{mA hg}^{-1}$ . For all the samples, the subsequent discharge and charge curves showed similar shape suggesting that the first cycle allowed to activate the electrode.

The cells were subsequently left for prolonged cycles under  $100 \text{ mA g}^{-1}$ . Overall, the capacity slightly decreases upon cycling. The solid prepared for 5 min presents the highest capacity with

$510 \text{ mAh g}^{-1}$  measured after 50 cycles. As shown in **Figure 8**, the solids prepared at  $t > 5 \text{ min}$  present lower capacities.

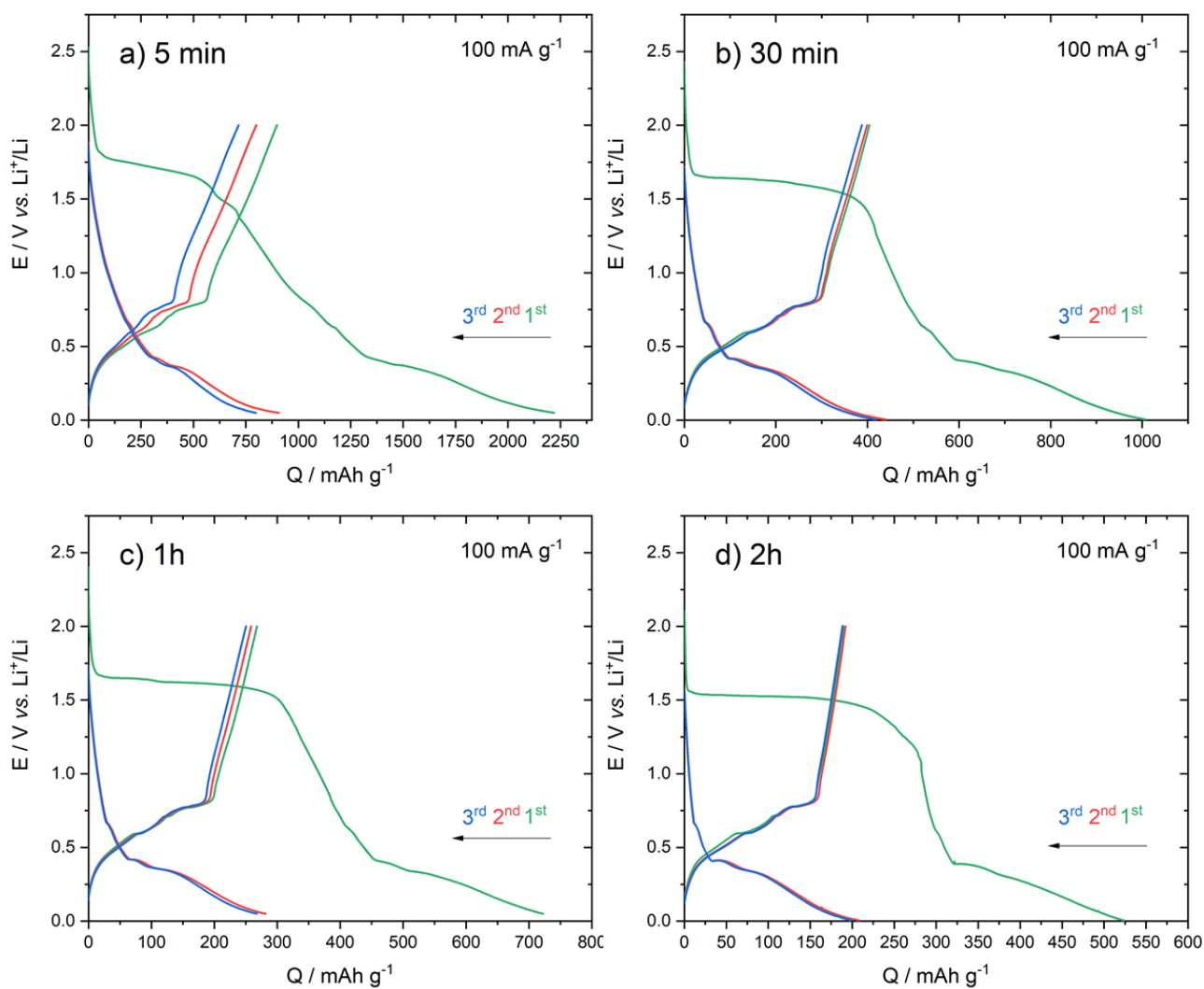


**Figure 7.** Galvanostatic discharge/charge curves obtained for the first three cycles on the series of electrodeposited samples. a) 5 min, b) 30 min, c) 1 h and d) 2 h. The cells were cycled under  $100 \text{ mA g}^{-1}$  between 0.05 and 2.0 V vs.  $\text{Li}^+/\text{Li}$ .

To determine the rate performance of this electrode material, C rate was increased stepwise from C/10 to 5C and then decreased to C/10, and cycled for 10 cycles at each rate (**Figure S8**). The best performing electrode is the thinnest at any rate, which correlated well with the high increase of lithium storage capacity with decrease of Sn mass. At high rate of 5C, 33% of the total capacity is recovered for the thinnest deposit. It was observed that this recovery of the total capacity increase either because the mass of deposited Sn decrease (25% for the thickest deposit) or because of the improve retention capacity brought by Cu-Sn alloys.

The difference in electrochemical properties for the series of samples can be related to two interconnected factors that are the particles morphology and the composition. A less dense film will allow to better accommodate the volume expansion experienced during the insertion/de-insertion reactions of lithium. Moreover, as compare to  $\beta$ -Sn, Cu-Sn alloys benefit from a lower volume expansion upon reactions with lithium.

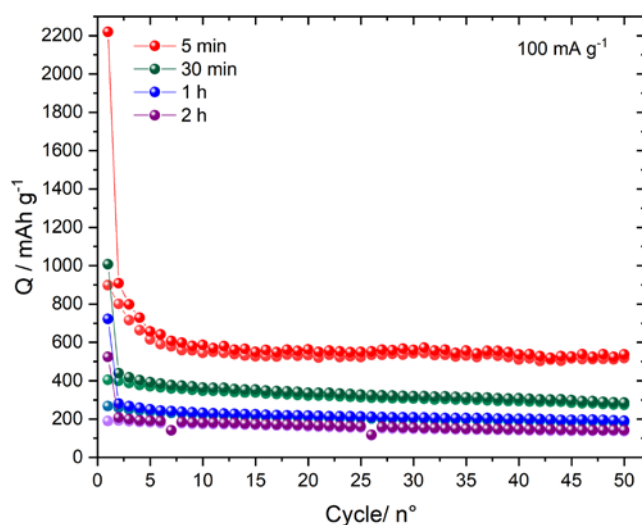


**Figure 8.** Long term cycling of the electrodeposited samples. The cells were cycled under  $100 \text{ mA g}^{-1}$  between 0.05 and 2.0 V vs. Li<sup>+</sup>/Li.

The evolution of the morphology after cycling was compared between the deposited samples obtained after 5 min and 1h (**Figure 9**). The first sample featuring the less dense structure allowed to better accommodate the volume variation by preserving the porous structure. After cycling, the sample prepared for 1h became much more compact which probably induced a blocking effect toward the lower part of the electrode.

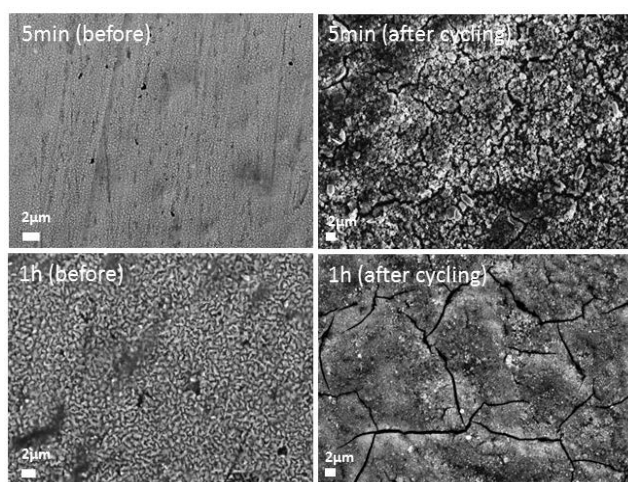


**Figure 9.** Scanning electron micrographs of electrodeposited samples (after 5 min and 1h) on Cu substrate before and after 50 cycles vs. Li<sup>+</sup>/Li.

## Conclusions

We investigated the electrodeposition of Sn using soluble Sn precursor based on TFSI<sup>-</sup> counter ion dissolved in [EMIm<sup>+</sup>][TFSI<sup>-</sup>] ionic liquid. The electrochemical behaviour of the Sn-ionic liquid solution was characterized by cyclic voltammetry using either inert (Mo) or reactive substrate (Cu). The diffusion coefficient of Sn<sup>2+</sup> in Mo electrode was found to be 1.61x10<sup>-8</sup> cm<sup>2</sup> s<sup>-1</sup> which is comparable to values obtained with other type of ionic liquids. The electrodeposition onto Cu led to the formation of a Cu-Sn alloy that was η-Cu<sub>6</sub>Sn<sub>5</sub> phase as identified by X-ray and electron diffraction. By analysing a FIB cross section on electrodeposited sample, we emphasized the interdiffusion of Cu and Sn atoms without any evidence of epitaxial growth. When prolonging the electrodeposition time, Cu atoms could no longer reach the upper surface favouring the formation of β-Sn. Tuning the reaction duration times enabled to tune the proportions of β-Sn/η-Cu<sub>6</sub>Sn<sub>5</sub>. The electrochemical properties of the binder and carbon-free electrodes were investigated in lithium coin cells. Increasing the mass of deposited sample degraded the capacity and reversibility of the system which was explained by a lower ability to accommodate the volume variation occurring during the electrochemical lithiation/delithiation process. This work is likely to be relevant to other types of elements providing similar salts.

## Conflicts of interest

There are no conflicts to declare.

## Acknowledgements

O.L acknowledges the “Agence Nationale de la Recherche (ANR)” in the framework of the “Investissements d’Avenir” with the reference “ANR-11-EQPX-0020” (GENESIS EQUIPEX) for the financial support that allowed the acquisition of the FIB system (HELIOS Nanolab 600 from FEI) for TEM sample preparations.

## References

- 1 I. A. Courtney and J. R. Dahn, *J. Electrochem. Soc.*, 1997, **144**, 2045–2052.
- 2 Y. Idota, T. Kubota, A. Matsufuji, Y. Maekawa and T. Miyasaka, *Science*, 1997, **276**, 1395–1397.
- 3 M. Winter and J. O. Besenhard, *Electrochim. Acta*, 1999, **45**, 31–50.
- 4 P. G. Bruce, B. Scrosati and J.-M. Tarascon, *Angew. Chemie Int. Ed.*, **47**, 2930–2946.
- 5 D. Larcher, S. Beattie, M. Morcrette, K. Edström, J.-C. Jumas and J.-M. Tarascon, *J. Mater. Chem.*, 2007, **17**, 3759–3772.
- 6 J. Hassoun, G. Derrien, S. Panero and B. Scrosati, *Adv. Mater.*, 2008, **20**, 3169–3175.
- 7 G. Derrien, J. Hassoun, S. Panero and B. Scrosati, *Adv. Mater.*, 2007, **19**, 2336–2340.
- 8 H. Groult, H. El Ghallali, A. Barhoun, E. Briot, L. Perrigaud, S. Hernandez and F. Lantelme, *Electrochim. Acta*, 2010, **55**, 1926–1932.
- 9 O. Mao and J. R. Dahn, *J. Electrochem. Soc.*, 1999, **146**, 423–427.
- 10 J. Hassoun, S. Panero, P. Simon, P. L. Taberna and B. Scrosati, *Adv. Mater.*, 2007, **19**, 1632–1635.
- 11 K. D. Kepler, J. T. Vaughey and M. M. Thackeray, *Electrochem. Solid-State Lett.*, 1999, **2**, 307–309.
- 12 H. Mukaibo, T. Sumi, T. Yokoshima, T. Momma and T. Osaka, *Electrochem. Solid-State Lett.*, 2003, **6**, A218–A220.
- 13 A. Lahiri and F. Endres, *J. Electrochem. Soc.*, 2017, **164**, D597–D612
- 14 F. C. Walsh and C. T. J. Low, *Surf. Coatings Technol.*, 2016, **304**, 246–262.
- 15 E. Frank, *ChemPhysChem*, 2002, **3**, 144–154.
- 16 A. P. Abbott and K. J. McKenzie, *Phys. Chem. Chem. Phys.*, 2006, **8**, 4265–4279.
- 17 F. C. Walsh and C. T. J. Low, *Surf. Coatings Technol.*, 2016, **288**, 79–94.
- 18 M. Morimitsu, Y. Nakahara and M. Matsunaga, *Electrochemistry*, 2005, **73**, 754–757.
- 19 N. Tachikawa, N. Serizawa, Y. Katayama and T. Miura, *Electrochim. Acta*, 2008, **53**, 6530–6534.
- 20 Y. S. Fung and D. R. Zhu, *J. Electrochem. Soc.*, 2002, **149**, A319–A324.
- 21 D. Zhu, H. Sun and Y. Fung, *ECS Trans.*, 2007, **3**, 239–248.
- 22 J.-F. Huang and I.-W. Sun, *J. Electrochem. Soc.*, 2003, **150**, E299–E306.
- 23 L. Anicai, A. Petica, S. Costovici, P. Prioteasa and T. Visan, *Electrochim. Acta*, 2013, **114**, 868–877.
- 24 A. Lahiri, G. Pulletikurthi, S. Abedin and F. Endres, *J. Solid State Electrochem.*, 2015, **19**, 785–793.
- 25 T.-I. Leong, Y.-T. Hsieh and I.-W. Sun, *Electrochim. Acta*, 2011, **56**, 3941–3946.
- 26 P. Giridhar, A. M. Elbasiony, S. Zein El Abedin and F. Endres, *ChemElectroChem*, 2014, **1**, 1549–1556.
- 27 D. Liu, H. Groult, L. Gaillon, C. Rizzi, N. Soulmi, C. M. Julien, E. Briot and D. Krulic, *J. Solid State Electrochem.*, 2015, **19**, 2517–2532.
- 28 R. Al-Salman, H. Sommer, T. Brezesinski and J. Janek, *Chem. Mater.*, 2015, **27**, 3830–3837.
- 29 X. Xie, X. Zou, K. Zheng, S. Wang, X. Lu, Q. Xu, and Z. Zhou, *J. Electrochem. Soc.*, 2017, **164**, D945–D953.

- 30 B. C. M. Martindale, S. E. W. Jones and R. G. Compton, *Phys. Chem. Chem. Phys.*, 2010, **12**, 1827–1833.
- 31 M.-J. Deng, P.-Y. Chen, T.-I. Leong, I.-W. Sun, J.-K. Chang and W.-T. Tsai, *Electrochem. commun.*, 2008, **10**, 213–216.
- 32 D. R. MacFarlane, J. Golding, S. Forsyth, M. Forsyth and G. B. Deacon, *Chem. Commun.*, 2001, 1430–1431.
- 33 D. R. MacFarlane, S. A. Forsyth, J. Golding and G. B. Deacon, *Green Chem.*, 2002, **4**, 444–448.
- 34 N. Soulmî, D. Dambournet, C. Rizzi, J. Sirieix-Plénet, M. Duttine, A. Wattiaux, J. Swiatowska, O. J. Borkiewicz, H. Groult and L. Gaillon, *Inorg. Chem.*, 2017, **56**, 10099–10106.
- 35 N. N. Acharya and P. G. Mukunda, *Metallography*, 1988, **21**, 137–150.
- 36 S. Fürtauer, D. Li, D. Cupid and H. Flandorfer, *Intermetallics*, 2013, **34**, 142–147.
- 37 D. Li, P. Franke, S. Fürtauer, D. Cupid and H. Flandorfer, *Intermetallics*, 2013, **34**, 148–158.
- 38 H. El Ghallali, H. Groult, A. Barhoun, K. Draoui, D. Krulic and F. Lantelme, *Electrochim. Acta*, 2009, **54**, 3152–3160.
- 39 D. Krulic, N. Fatouros and D. Liu, *J. Electroanal. Chem.*, 2015, **754**, 30–39.
- 40 D. Liu, D. Krulic, H. Groult and N. Fatouros, *J. Electroanal. Chem.*, 2016, **775**, 91–104.
- 41 D. J. Schiffrin, *J. Electroanal. Chem. Interfacial Electrochem.*, 1986, **201**, 199–203.
- 42 T. Berzins and P. Delahay, *J. Am. Chem. Soc.*, 1953, **75**, 555–559.
- 43 Y. NuLi, J. Yang and P. Wang, *Appl. Surf. Sci.*, 2006, **252**, 8086–8090.
- 44 M. Guo, X. Zhang, W. Meng, X. Liu, G. Wang, Z. Bai, Z. Wang, F. Yang, *Solid state ionics*, 2018, **325**, 120–127.
- 45 R. Z. Hu, M. Q. Zeng, M. Zhu, *Electrochim. Acta*, 2009, **54**, 2843–2850.
- 46 H. Algul, M. Uysal, M. Toku, S. Ozcan, T. Cetinkaya, H. Akbulut, A. Alp, *Int. J. Hydrogen Energy*, 2016, **41**, 9819–9827.
- 47 G. F. Ortiz, M. C. Lopez, R. Alcantara, J. L. Tirado, *J. Alloys Compd*, 2014, **585**, 331–336;
- 48 P. Antitomaso, B. Fraisse, L. Stievano, S. Biscaglia, D. Aymé-Perrot, P. Girard, M. T. Sougrati, L. Monconduit, *J. Mat. Chem. A*, 2017, **5**, 6546–6555
- 49 J.-S. Bridel, S. Grugeon, S. Laruelle, J. Hassoun, P. Reale, B. Scrosati and J.-M. Tarascon, *J. Power Sources*, 2010, **195**, 2036–2043.

## Supporting Information

### *Sn(TFSI)<sub>2</sub> as Suitable Salt For the Electrodeposition of Nanostructured Cu<sub>6</sub>Sn<sub>5</sub>-Sn Composite obtained on Cu electrode in Ionic Liquid*

Nadia Soulmi<sup>a</sup>, Ana-Gabriela Porras-Gutierrez<sup>\*a</sup>, Mordvinova Natalia<sup>b</sup>, Oleg Lebedev<sup>b</sup>, Cécile Rizzi<sup>a,c</sup>, Juliette Sirieix-Plénet<sup>a,c</sup>, Henri Groult<sup>a,c</sup>, Damien Dambournet<sup>a,c</sup> and Laurent Gaillon<sup>\*a,c</sup>

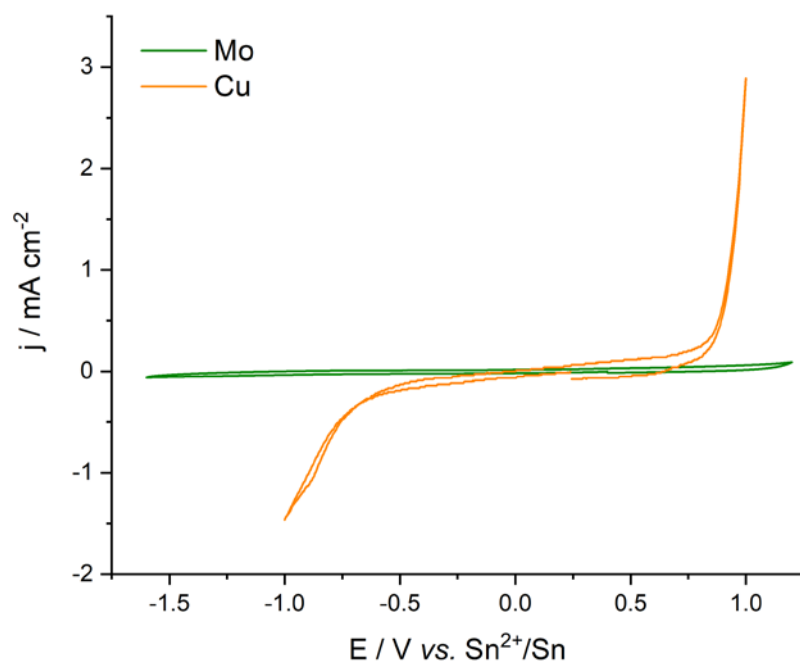


**Figure S1.** Cyclic voltammetry in [EMIm<sup>+</sup>][TFSI<sup>-</sup>] ionic liquid on Mo and Cu electrodes at a scan rate of 0.05 V s<sup>-1</sup>.

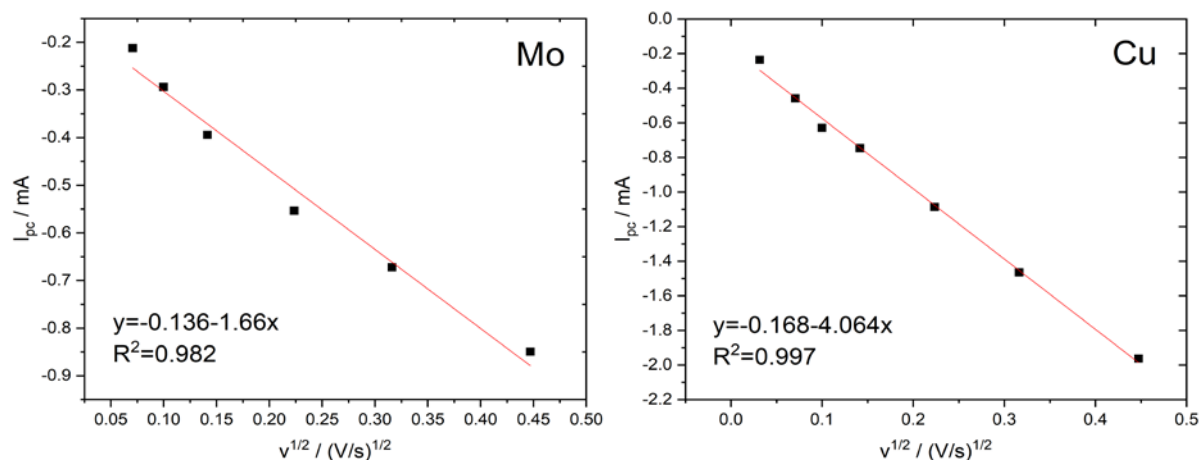


**Figure S2.** Variation of  $I_{pc}=f(v^{1/2})$  obtained by cyclic voltammetry at different scan rates, in 25 mM Sn(TFSI)<sub>2</sub> in [EMIm<sup>+</sup>][TFSI<sup>-</sup>] solution with Mo and Cu electrodes.

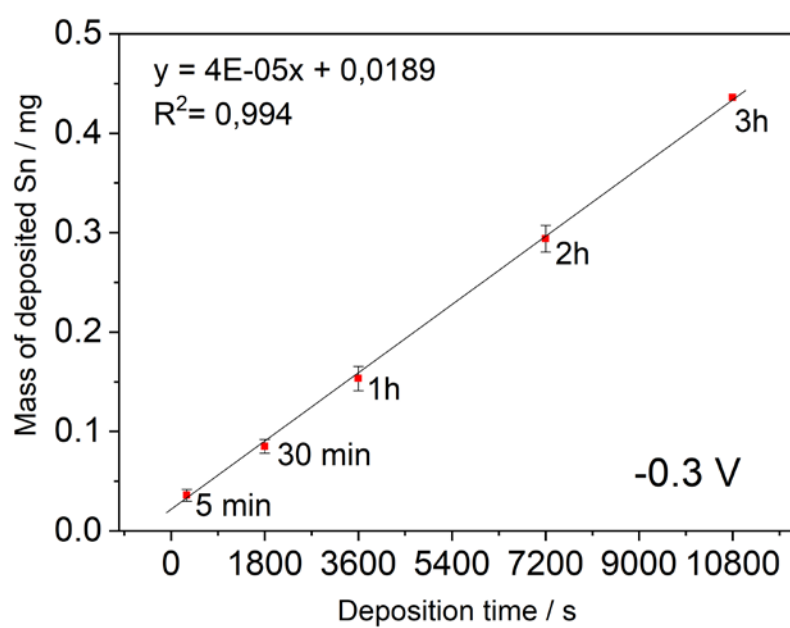


**Figure S3.** Variation of the mass of Sn deposited on Cu substrate in function of the deposition time at -0.3 V.



**Figure S4.** Images of the electrodes after different deposition time on Cu substrate.